SUPPLEMENTARY INFORMATION
DOI: 10.1038/s41551-017-0139-0

nature biomedical engineering

In the format provided by the authors and unedited.

Corrected: Publisher correction

Whole-tissue biopsy phenotyping of three-dimensional tumours reveals patterns of cancer heterogeneity

Nobuyuki Tanaka[1,2], Shigeaki Kanatani[1], Raju Tomer[3], Cecilia Sahlgren[4,5], Pauliina Kronqvist[6], Dagmara Kaczynska[1], Lauri Louhivuori[1], Lorand Kis[7,8], Claes Lindh[7,8], Przemysław Mitura[9], Andrzej Stepulak[10], Sara Corvigno[7], Johan Hartman[7,8], Patrick Micke[11], Artur Mezheyeuski[7], Carina Strell[7], Joseph W. Carlson[7,8], Carlos Fernández Moro[12,13], Hanna Dahlstrand[7,11,14], Arne Östman[7], Kazuhiro Matsumoto[2], Peter Wiklund[15,16], Mototsugu Oya[2], Ayako Miyakawa[1,15,16], Karl Deisseroth[17,18,19] and Per Uhlén[1]*

[1]Department of Medical Biochemistry and Biophysics, Karolinska Institutet, SE-17177 Stockholm, Sweden. [2]Department of Urology, Keio University School of Medicine, Tokyo 160-8582, Japan. [3]Department of Biological Sciences, Columbia University, New York, NY 10027, USA. [4]Turku Centre for Biotechnology, University of Turku and Faculty of Science and Engineering, Åbo Akademi University, FI-20521 Turku, Finland. [5]Institute for Complex Molecular Systems, Eindhoven University of Technology, Eindhoven, MB 5600, The Netherlands. [6]Institute of Biomedicine/Pathology, University of Turku, FI-20014 Turku, Finland. [7]Department of Oncology-Pathology, Karolinska Institutet, SE-17176 Stockholm, Sweden. [8]Department of Pathology and Cytology, Karolinska University Hospital, SE-17176 Stockholm, Sweden. [9]Department of Urology and Oncological Urology, Medical University in Lublin, ul. Jaczewskiego 8, 20-954 Lublin, Poland. [10]Department of Biochemistry and Molecular Biology, Medical University in Lublin, ul. Chodzki 1, 20-093 Lublin, Poland. [11]Department of Immunology, Genetics and Pathology, Uppsala University, SE-75185 Uppsala, Sweden. [12]Department of Laboratory Medicine, Division of Pathology, Karolinska Institutet, Karolinska University Hospital, SE-14186 Stockholm, Sweden. [13]Department of Clinical Pathology/Cytology, Karolinska University Hospital, SE-14186 Stockholm, Sweden. [14]Department of Oncology-Pathology, Karolinska University Hospital, SE-17176 Stockholm, Sweden. [15]Department of Molecular Medicine and Surgery, Karolinska Institutet, SE-17177 Stockholm, Sweden. [16]Department of Urology, Karolinska University Hospital, SE-17176 Stockholm, Sweden. [17]Howard Hughes Medical Institute, W080 Clark Center, Stanford University, 318 Campus Drive West, Stanford, CA 94305, USA. [18]Department of Bioengineering, W080 Clark Center, Stanford University, 318 Campus Drive West, Stanford, CA 94305, USA. [19]Department of Psychiatry and Behavioral Sciences, W080 Clark Center, Stanford University, 318 Campus Drive West, Stanford, CA 94305, USA. Nobuyuki Tanaka and Shigeaki Kanatani contributed equally to this work. *e-mail: per.uhlen@ki.se

Supplementary Information (SI)

Table of contents

Supplementary Figures 2
Supplementary Figure 1. ..... **2**
Supplementary Figure 2 ..... **3**
Supplementary Figure 3 ..... **4**
Supplementary Figure 4 ..... **5**
Supplementary Figure 5 ..... **6**
Supplementary Figure 6 ..... **6**
Supplementary Figure 7 ..... **7**
Supplementary Figure 8 ..... **8**
Supplementary Figure 9 ..... **8**
Supplementary Tables 9
Supplementary Table 1 ..... **9**
Supplementary Table 2 ..... **9**
Supplementary Table 3 ..... **9**
Supplementary Table 4 ..... **10**
Supplementary Table 5 ..... **10**
Supplementary Video legends 11
Supplementary Video 1 ..... **11**
Supplementary Video 2 ..... **11**
Supplementary Video 3 ..... **11**
Supplementary Video 4 ..... **11**
Supplementary Video 5 ..... **11**

Supplementary Figures

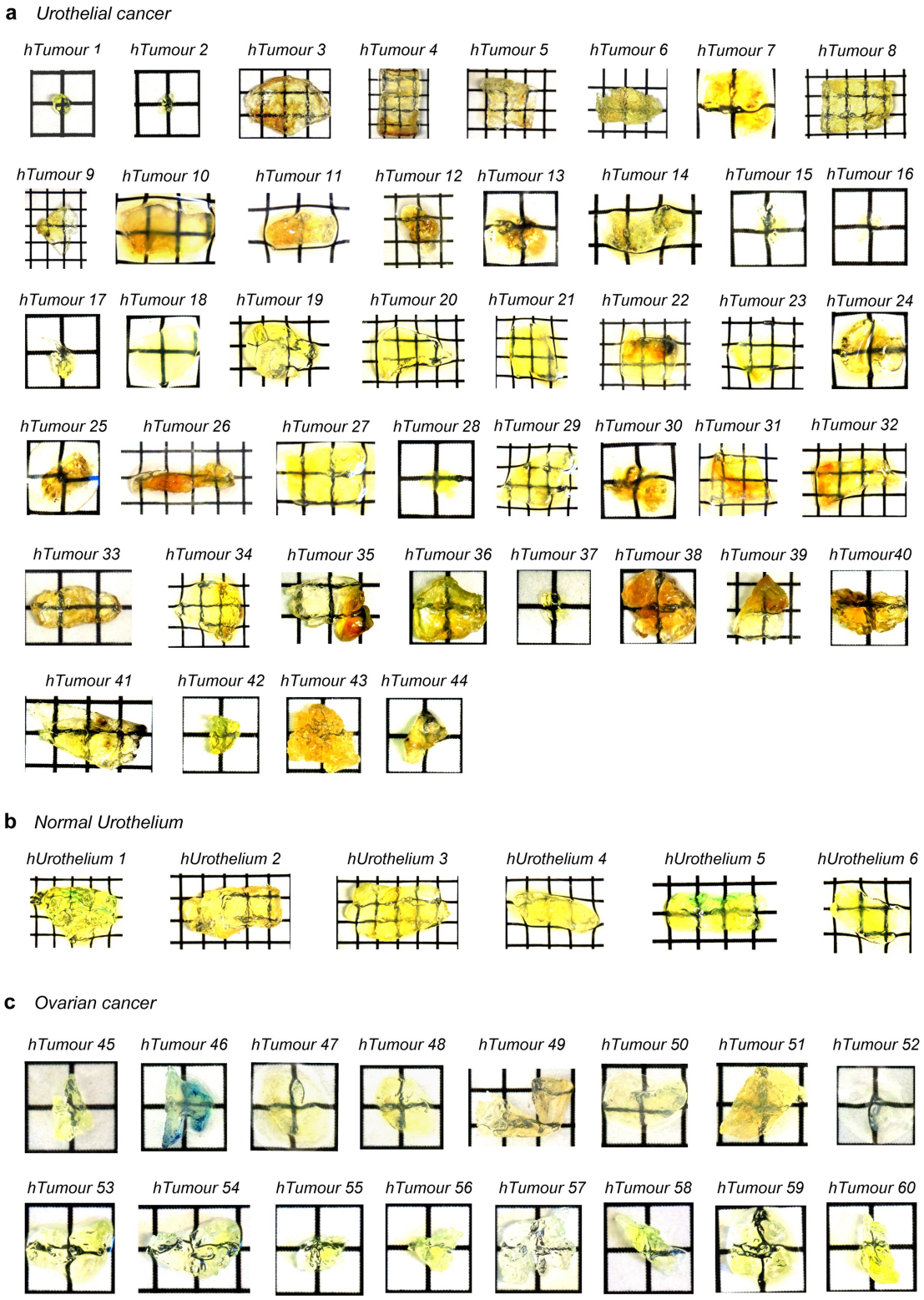

Supplementary Figure 1. Cleared human FFPE tissues. Images of 44 deparaffinized and cleared human FFPE urothelial tumours (**a**, hTumour 1-44), 6 normal urotheliums (**b**, hUrothelium 1-6), and 16 ovarian tumours (**c**, hTumour 45-60). The grid lines are separated by 3 mm.

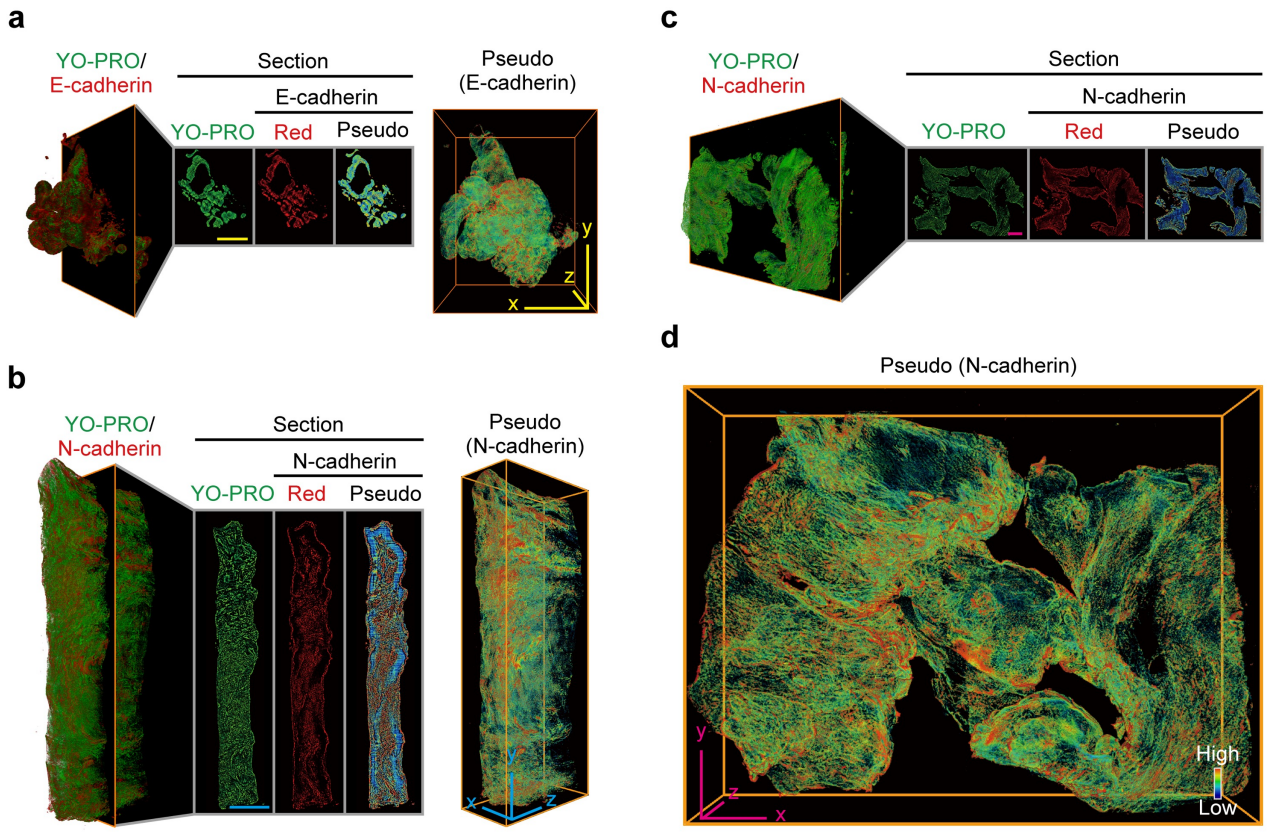

Supplementary Figure 2. Whole-tissue 3D imaging of human FFPE tumours. Volume rendering of 3D light-sheet microscopy data of human FFPE tumours immunolabeled for E-cadherin (**a**, hTumour 2) and N-cadherin (**b**, **c,** hTumour 4, hTumour 5). Pseudo-colours in **a** indicate E-cadherin and in **b**, **c** indicate N-cadherin low (blue) and high (red) expression. (**d**) Volume rendering of hTumour 5 immunolabeled for N-cadherin, coded in pseudo colours. Scale bars and x,y,z-indicators, 600 µm (yellow), 1200 µm (magenta), 1800 µm (cyan).

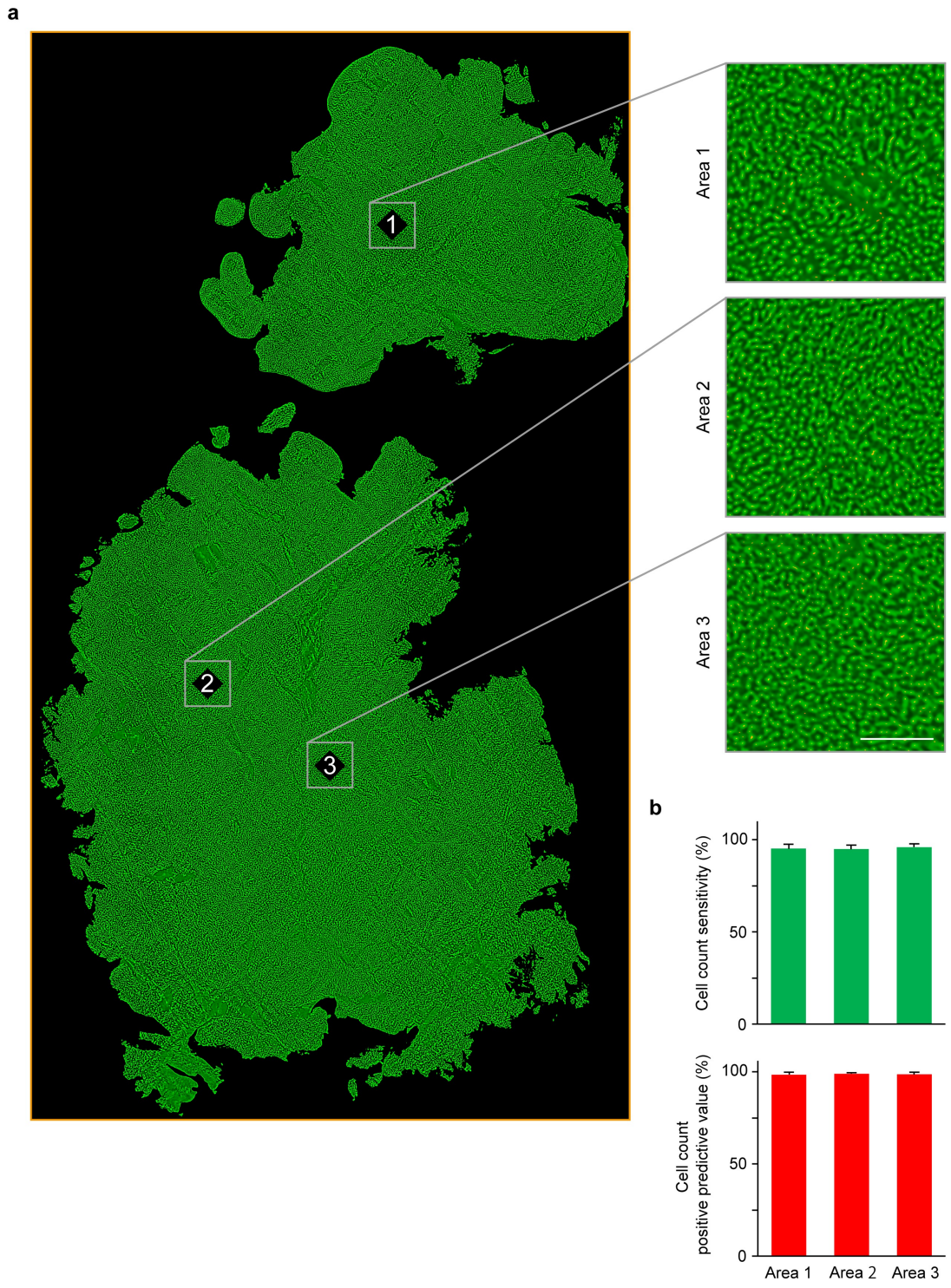

Supplementary Figure 3. Single-cell analysis using the DIPCO pipeline. (**a**) Image of FFPE tumour (hTumour 7) stained for nuclei with YO-PRO (green). The high-magnification images (right-hand panels) resolve individual cells in boxed areas 1-3. (**b**) Histograms showing the accuracies of cell count sensitivity (green) and cell count positive predicted value (red) (see Methods). Data are mean ± s.e.m. Scale bars, 100 µm.

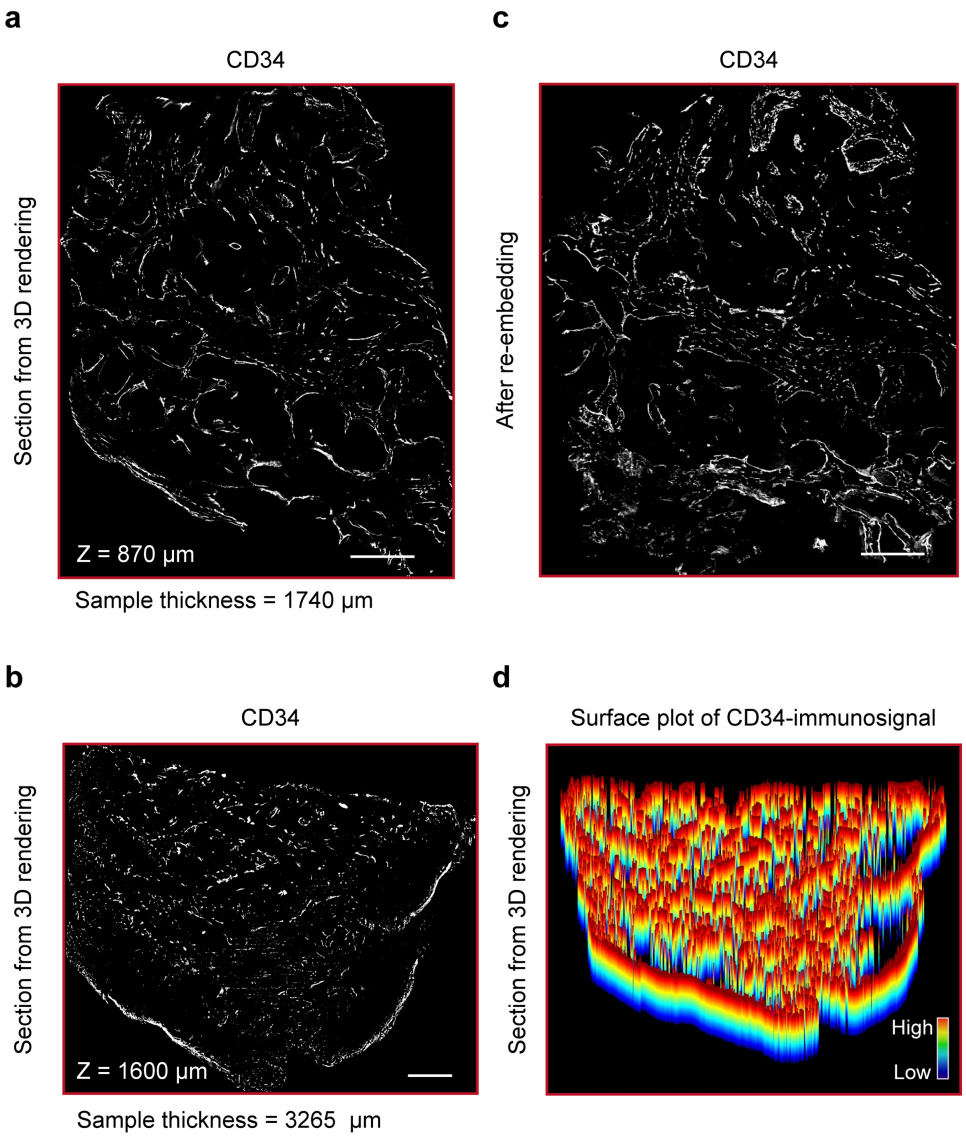

Supplementary Figure 4. Assessment of antibody penetration and light scattering using the DIPCO pipeline. Images of CD34 immunostained FFPE tumours of thicknesses 1740 µm (**a, c**) and 3265 µm (**b, d**). The image in **a** shows a section from the centre of a 3D image of hTumour 27 (thickness 1740 µm) recorded using the DIPCO pipeline and the image in **c** shows a section recorded by physically cutting the tumour depicted in **a** at the centre after re-embedding and examining the surface after re-staining using 2D fluorescence microscopy. The image in **b** shows a section from the centre of a 3D image of hTumour 34 (thickness 3265 µm) recorded using the DIPCO pipeline and the image in **d** shows a surface plot of the immunosignal depicted in **b**. The surface plot was generated using the mesh function in MATLAB. Scale bars, 1000 µm.

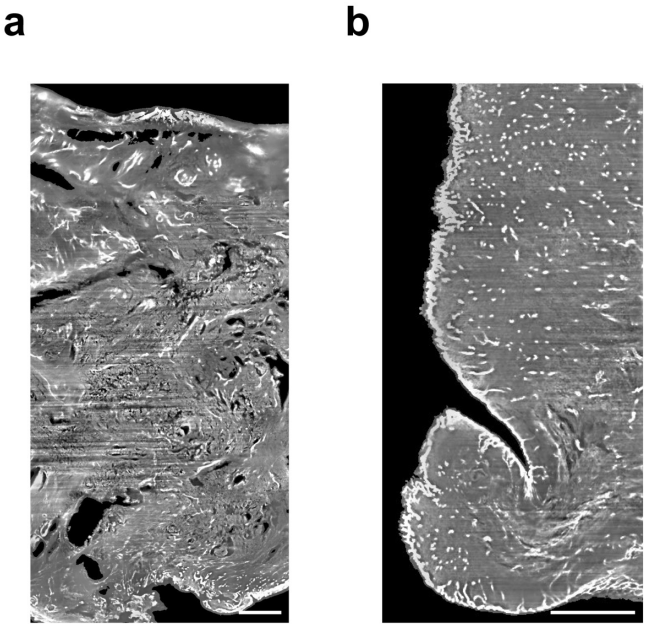

Supplementary Figure 5. Assessment of vessel heterogeneity between tumour and normal tissue. (**a**) Urinary bladder cancer (hTumour 34) and (**b**) normal urothelial tissue (hUrothelium 6) immunostained for CD34. Scale bars, 500 µm.

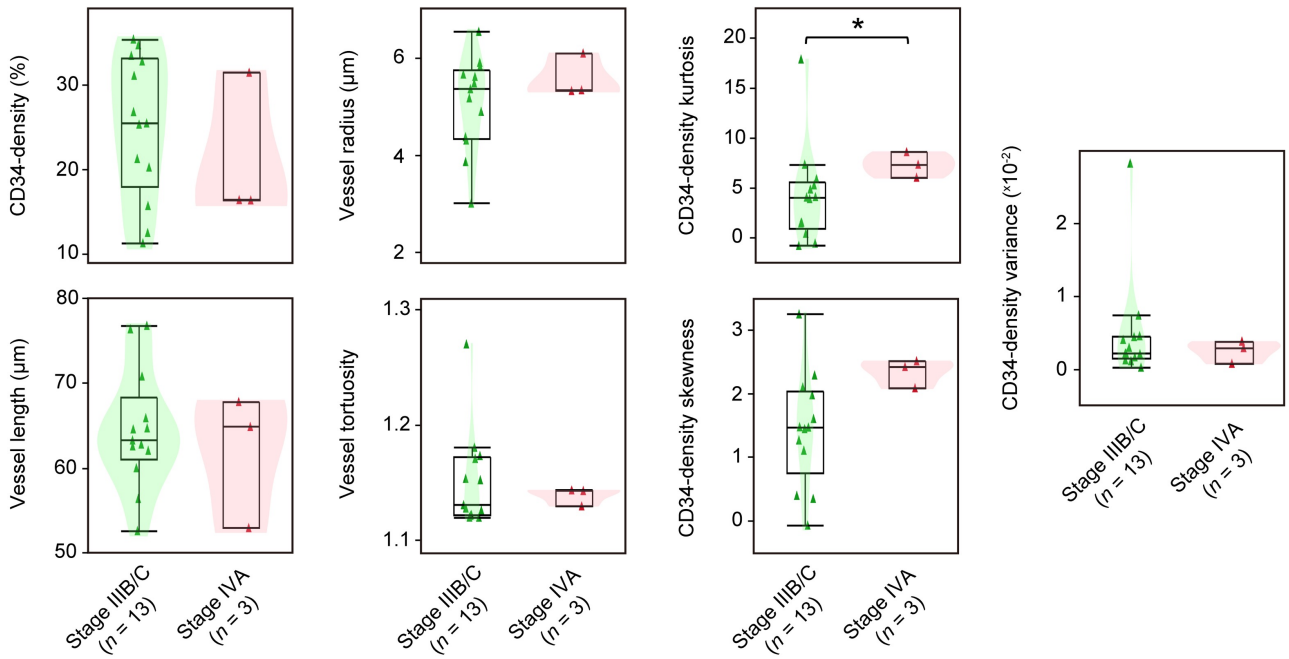

Supplementary Figure 6. Diagnostic evaluation of clinical ovarian cancer FFPE samples using the DIPCO pipeline. Violin and box plots of vascular attributes from sixteen human samples of stage IIIB/C or stage IVA ovarian cancer, measured with the DIPCO pipeline. The line within the box is the median. The upper and lower ends of the box are the upper and lower quartiles, and the bars are the minimum and maximum values. *$P < 0.05$ by the two-tailed Mann-Whitney *U*-test.

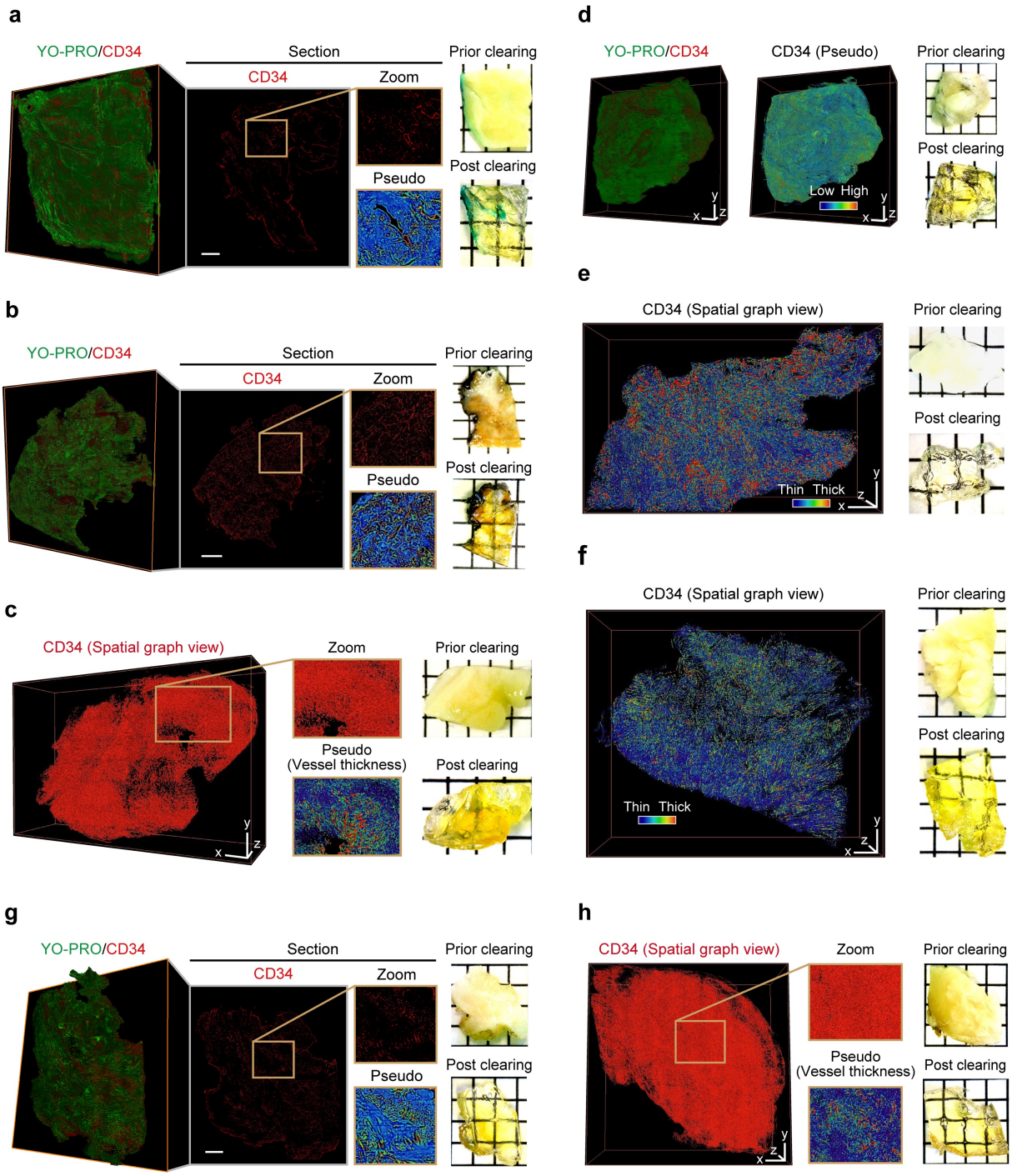

Supplementary Figure 7. 3D imaging of vasculature in various types of cancers using the DIPCO pipeline. Volume rendering of light-sheet microscopy data of CD34 immunolabeled pancreas cancer (**a**, hTumour 61), liver metastasis from pancreas cancer (**b**, hTumour 62), pancreas cancer (**c**, hTumour 63), lung cancer (**d**, hTumour 64), colon cancer (**e**, hTumour 65), colon benign polyp (**f**, hPolyp), thyroid cancer (**g**, hTumour 66), and tonsil cancer (**h**, hTumour 67). Pseudo-colours in **a**, **b**, **d**, and **g** indicate low (blue) and high (red) CD34 expression. Pseudo-colours in **c**, **e**, **f**, and **h** indicate thin (blue) and thick (red) blood vessels. The whole-tissue bright-field images are of deparaffinized FFPE samples prior and post clearing. The grid lines are separated by 3 mm. Scale bars and x,y,z-indicators, 1000 µm.

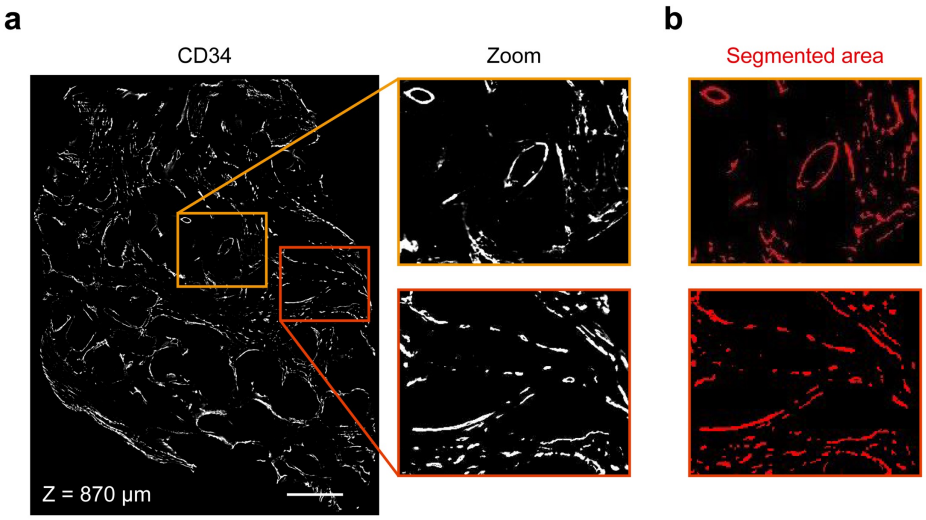

Supplementary Figure 8. Assessment of blood vessel segmentation with the DIPCO pipeline. (**a**) Image of FFPE tumour (hTumour 27) immunostained for CD34 at z-depth 870 µm. The high-magnification images (right-hand panels) are of boxed areas. (**b**) Segmented areas of boxed regions in **a** assessed using an intensity-based threshold of the CD34 immunosignal. Scale bar, 1000 µm.

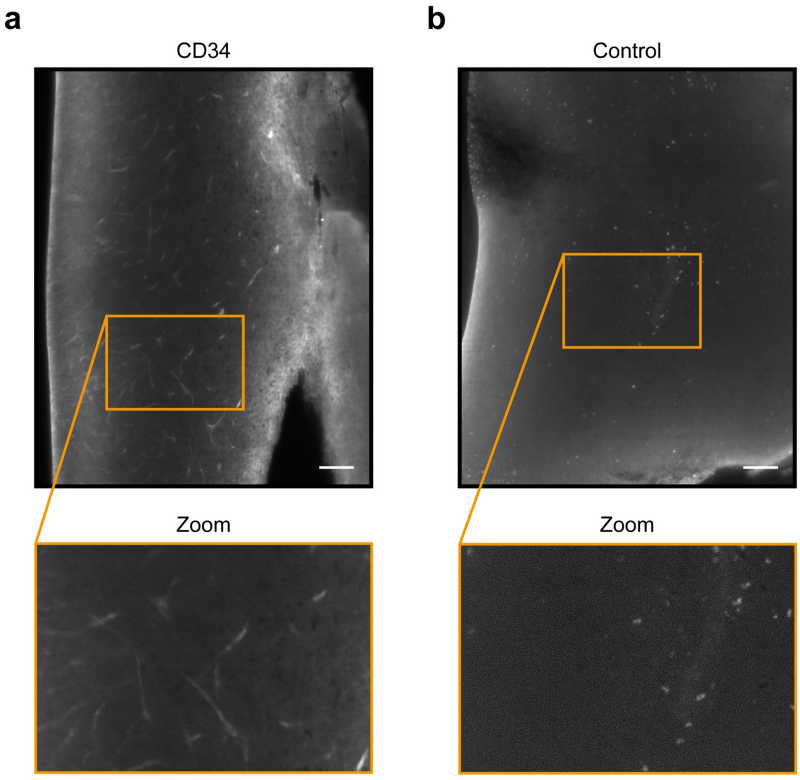

Supplementary Figure 9. 3D histological study of mouse bladder tumour using the DIPCO pipeline. Raw unprocessed images of mouse orthotopic bladder tumours immunostained for CD34 (**a**) or secondary antibody only (**b**). The high-magnification images (lower panels) are of boxed areas. Scale bars, 100 µm.

Supplementary Tables

Supplementary Table 1. Clinicopathological characteristics in 50 human urothelial FFPE samples

(Excel file 16 KB).

Supplementary Table 2. Clinicopathological characteristics in 16 human ovarian cancer FFPE samples

(Excel file 12 KB).

Supplementary Table 3. Parameters associated with muscle-invasive urothelial tumours after adjusting for univariate and multivariate logistic regression

	Univariate	Multivariate		
Parameter	***P* value**	***P* value**	**Odds ratio**	**95% CI**
2D imaging				
CD34-density (2D)	0.710			
3D imaging				
Vessel length	0.710			
CD34-density variance	0.979			
CD34-density skewness	0.285			
CD34-density	0.084			
Vessel tortuosity	0.049			
CD34-density kurtosis	0.042	0.028	1.352	1.033 - 1.769
Vessel radius	0.014	0.008	3.523	1.381 - 8.988

Abbreviation: CI, confidence interval.

Supplementary Table 4. Comparison of the ROC-AUC analysis values between 2D imaging and 3D imaging data analysis

Parameter	AUC (95% CI)	*P* value
2D imaging		
CD34-density (2D)	0.547 (0.362-0.733)	-
3D imaging		
Vessel length	0.524 (0.334-0.713)	0.871
CD34-density variance	0.537 (0.279-0.647)	0.941
CD34-density skewness	0.587 (0.398-0.776)	0.779
CD34-density	0.642 (0.467-0.817)	0.331
Vessel tortuosity	0.653 (0.478-0.827)	0.359
CD34-density kurtosis	0.661 (0.487-0.834)	0.428
Vessel radius	0.753 (0.592-0.913)	0.057
3D multi-parameter model	0.839 (0.711-0.968)	0.009

Abbreviation: AUC, area under the curve; CI, confidence interval, *P* value from the DeLong test, compared with CD34-density (2D).

Supplementary Table 5. Antibodies tested post re-embedding

Antigen	Vendor	Reference
Ki-67	Abcam	ab15580
p53	Santa Cruz	sc-6243
p21	Cell Signaling Technology	#2947
p27	Abcam	ab32034
Cyclin E	Santa Cruz	sc-198
Caspase 3	Cell Signaling Technology	#9661
Survivin	Abcam	ab76424
Bcl-2	Abcam	ab32124
FGFR3	Santa Cruz	sc-123
4E-BP1	Cell Signaling Technology	#9644
ER-α	Santa Cruz	sc-543
AR	Santa Cruz	sc-816
CD44	Abcam	ab157107
CD34	Abcam	ab8536
HIF1-α	Novus Biologics	NB100-479

Supplementary Video legends

Supplementary Video 1. Three-dimensional volume reconstruction of hTumour 1 (see Fig. 3a) immunostained for E-cadherin. The nuclei were stained with YO-PRO.
Bounding box (x,y,z), 1.91, 1.52, 0.80 mm.
(mp-4 file 92.8 MB)

Supplementary Video 2. Three-dimensional volume reconstruction of hTumour 3 (see Fig. 3b) immunostained for N-cadherin. The nuclei were stained with YO-PRO.
Bounding box (x,y,z), 8.00, 9.90, 1.65 mm.
(mp-4 file 84.3 MB)

Supplementary Video 3. Three-dimensional volume reconstruction of hTumour 6 (see Fig. 3c) immunostained for CD34.
Bounding box (x,y,z), 4.70, 2.70, 1.65 mm.
(mp-4 file 28.1 MB)

Supplementary Video 4. Three-dimensional volume reconstruction of the CD34 signal presented in Supplementary Video 3, processed to outline the vascular network. Pseudo-colouring depicts vessel thicknesses. The nuclei were stained with YO-PRO.
Bounding box (x,y,z), 4.70, 2.70, 1.65 mm.
(mp-4 file 103.8 MB)

Supplementary Video 5. Single-cell 3D volume reconstruction of hTumour 7 (see Fig. 4a) immunostained for Vimentin. Each sphere represents a single cell and the pseudo-colour scale indicates the Vimentin expression level. The total number of cells in hTumour 7 is 13,214,289.
Bounding box (x,y,z), 4.20, 7.60, 1.60 mm.
(mp-4 file 61.2 MB)